Title: Iron-sensing and redox properties of the hemerythrin-like domains of Arabidopsis BRUTUS and BRUTUS-LIKE2 proteins

Authors: Jacob Pullin[1], Jorge Rodríguez-Celma[2], Marina Franceschetti[1], Julia E A Mundy[1], Dimitri A Svistunenko[3], Justin M Bradley[4], Nick E Le Brun[4*]✉ and Janneke Balk[1,5*]✉

[1] Department of Biochemistry and Metabolism, John Innes Centre, Norwich NR4 7UH, UK
[2] Plant Biology Department, Estación Experimental de Aula Dei (EEAD), CSIC, 50059 Zaragoza, Spain
[3] School of Life Sciences, University of Essex, Colchester, Essex CO4 3SQ, UK
[4] Centre for Molecular and Structural Biochemistry, School of Chemistry, Pharmacy and Pharmacology, University of East Anglia, Norwich NR4 7TJ, UK
[5] School of Biological Sciences, University of East Anglia, Norwich NR4 7TJ, UK

* These authors jointly supervised the work
✉ n.le-brun@uea.ac.uk; janneke.balk@jic.ac.uk

ABSTRACT

Iron uptake in plants is negatively regulated by highly conserved hemerythrin (Hr) E3 ubiquitin ligases exemplified by *Arabidopsis thaliana* BRUTUS (BTS). Physiological studies suggest these are the elusive plant iron sensors, but biochemical evidence is lacking. Here we demonstrate that the N-terminal domains of BTS and BTS-LIKE2 (BTSL2) respectively bind three and two diiron centres within three closely packed Hr-like subdomains. The centres can be reversibly oxidized by O_2 and H_2O_2, resulting in a di-Fe^{3+} form that is non-labile. In the reduced state, a proportion of the iron becomes labile, based on accessibility to Fe^{2+} chelators and reconstitution experiments, consistent with dynamic iron binding. Impaired iron binding and altered redox properties in the BTS *dgl* variant correlate with diminished capacity to suppress the downstream signalling cascade. These data provide the biochemical foundation for a mechanistic model of how BTS/Ls function as iron sensors that are unique to the plant kingdom.

INTRODUCTION

The concentration of iron in cells and whole organisms is tightly controlled to meet demand while avoiding toxicity from redox cycling of free iron (Fenton chemistry). In plants, the uptake of iron is negatively regulated by specific E3 ubiquitin-protein ligases, known as Hemerythrin RING and Zinc-finger (HRZ) proteins in monocots, and named BRUTUS (BTS) in dicot species[1]. The related BTS-LIKE (BTSL) proteins are found in dicots only and have a specific role in regulating iron uptake in roots[2,3]. Mutations in the rice *HRZ* or Arabidopsis *BTS* genes result in accumulation of excessive amounts of iron, leading to embryo lethality in knockout alleles[4-6]. By contrast, Arabidopsis plants lacking expression of both the *BTSL1* and *BTSL2* genes are viable and accumulate moderate amounts of iron under certain growth conditions[2,3].

The HRZ/BTS proteins are relatively large (~140 kDa), consisting of consecutive hemerythrin -like sequences at the N-terminus and a RING-type ubiquitin ligase domain at the C-terminus (Fig. 1a). Despite their name, hemerythrins do not bind heme but a pair of cations, usually iron, and are subdivided into canonical O_2-carrying hemerythrins and hemerythrin (Hr)-like proteins based on the pattern of the metal-binding His and Glu residues[7]. The E3 ligase domain of HRZ/BTS interacts with transcription factors that orchestrate the iron-deficiency response and targets them for degradation[8,9] (and reviewed in [1]). Combination of a Hr-like sequence and E3 ligase is also found in the mammalian F-box/LRR-repeat protein 5 (FBXL5)[10,11], which has a single Hr-like sequence at the N-terminus and a subunit of a Cullin-type E3 ligase at the C-terminus. In the presence of iron and O_2, FBXL5 promotes interaction with Iron Regulatory Protein 2 (IRP2), followed by ubiquitination and degradation of IRP2[12]. By analogy, the Hr-like domain of HRZ/BTS has been proposed to sense iron and/or O_2, but no biochemical studies have been reported to date. Moreover, why there are three Hr-like sequences and how redox activity could influence ubiquitin ligase activity are open questions.

Here we report on the architecture, iron-binding properties and redox activity of the recombinantly expressed Hr-like domains of BTS and BTSL2 from Arabidopsis. Unexpectedly, SAXS analysis showed that the three Hr-like folds are tightly packed in a large, rigid domain, an arrangement supported by AlphaFold2 prediction. A range of spectroscopic methods showed that BTS and BTSL2 bind three and two diiron centres, respectively, which were strongly bound in the oxidized state, but partially labile upon reduction. Impaired iron binding and oxidation activity in vitro were correlated with decreased activity of BTS in vivo. These data suggest a model for the iron-sensing mechanism of BTS/L proteins by means of diiron centres in a unique triple Hr-like domain.

63 RESULTS

64 **The extended N-terminus with three Hr-like sequences is conserved in BTS/L proteins**
65 **throughout the green lineage**

66 Previous phylogenetic analyses identified HRZ/BTS homologues in different clades of the
67 green lineage, including green algae[1,4,13-15]. Similar to higher plants, the expression of algal
68 homologues is induced in response to iron deficiency in *Chlamydomonas reinhardtii*[13],
69 *Dunaliella* species and diatoms[15], suggesting that the role of HRZ/BTS in iron homeostasis is
70 highly conserved. While most HRZ/BTS protein sequences are predicted to have three
71 sequential Hr-like motifs, homologs with only one or two motifs were reportedly found in some
72 plant genomes using bioinformatics[14]. With the ever-expanding availability and completeness
73 of genome sequences, we revisited the phylogenetic analysis to investigate possible variation
74 in the number of Hr-like motifs. All major groups of angiosperms, ferns, mosses and algae
75 have at least one protein of 1200 - 1400 amino acid residues with 50 - 70% overall sequence
76 similarity to Arabidopsis BTS. The phylogenetic relationship of these proteins follows the
77 accepted evolution of the green lineage (Fig. 1a). All the investigated HRZ/BTS sequences
78 had an N-terminal sequence over 950 residues in length encompassing three distinct
79 sequences with a predicted alpha-helical bundle fold typical of Hr-like proteins. This included
80 sequences of HRZ2 in different rice cultivars, indicating that the previously reported open
81 reading frame with one Hr-like sequence was incomplete[4].

82 Gene duplication and functional specialization of *HRZ*/*BTS* genes have occurred at least
83 twice: Poaceae (grasses including cereal crops) harbour two *HRZ* paralogues (Fig. 1a). *HRZ1*
84 and *HRZ2* are very similar in sequence but are functionally non-redundant, as shown by
85 mutant studies in rice[4]. Eudicots including Arabidopsis have an additional monophyletic clade
86 of *BTSL* genes, encoding protein sequences that have diverged substantially from BTS (44%
87 similarity). Arabidopsis *BTSL1* and *BTSL2* have more specialized functions in regulating iron
88 uptake in roots[1,8], although the precise functional differences with *BTS* remain to be
89 established.

90 In the main HRZ/BTS clade, all three Hr-like sequences contain the diiron-binding motif H-
91 HxxxE-H-HxxxE (InterPro IPR012312). In the BTSL clade, the second sequence has an
92 incomplete H/E motif but is predicted to have the typical alpha-helical bundle fold, as
93 previously noted[1]. In some moss sequences, one of the six H/E residues is lacking or not well-
94 aligned (indicated by a question mark in Fig. 1a).

95

96

Models of the HRZ/BTS proteins generated using AlphaFold2 (see examples at www.uniprot.org) consistently showed that the three Hr-like folds are arranged in the order H2-H1-H3 with large contact surfaces between the folds. There is little interaction between the triple Hr-like domain and the E3 ligase domain, except for the direct connection with H3. The predicted structure was similar for the BTSL2 proteins, as depicted in Fig. 1b. This places the metal centres, if present, relatively close to one another (~21 Å apart) and arranged linearly.

The three Hr-like folds of BTSL2 form a single inflexible domain structure

To obtain experimental evidence for the AlphaFold2 model of the triple Hr-like domain, the N-terminal part of BTSL2 (BTSL2-N, amino acids 1 - 831) from *Arabidopsis thaliana* was produced in *Escherichia coli* for structural studies. The Maltose Binding Protein (MBP) coding sequence was cloned upstream to improve solubility and a Strep tag was added at the C-terminus for affinity purification (Fig. 2a). Following purification, the MBP-BTSL2-N fusion protein was cleaved with Factor Xa protease and the 98 kDa BTSL-N protein was re-isolated by size-exclusion chromatography (SEC) (Fig. 2b). Because crystallisation trials were unsuccessful, structural data were obtained through small-angle X-ray scattering (SAXS). This low-resolution technique provides information on the average size and shape of proteins in solution[17]. Scattering is measured as the protein elutes from a SEC column (SEC-SAXS) in a series of frames, to enable the selection of the highest quality data, avoiding misfolded and aggregated protein in the sample.

Four frames in the middle of the single elution peak (Supplementary Fig. 1a) were selected and merged to give the scattering profile of intensity (I) as a function of q, the momentum transfer variable (Fig. 2c). The shape of the profile was typical of non-spherical monodispersed particles[17]. Plotting the natural logarithm of intensity, ln(I), versus the square of lower q values, known as Guinier analysis, gave a straight line which confirmed the homogeneity of the sample (Fig. 2c, inset). The slope of the Guinier plot was used to calculate a radius of gyration R_g of 33.95 ± 0.05 Å. The Bayesian inference method[18] gave a molecular mass of 101 kDa, which is close to the expected molecular mass of 97.771 kDa calculated from the amino acid sequence (Supplementary Data 1) and shows that the recombinant protein is monomeric. The shape of the Kratky plot of $q^2 \times I$ versus q (Supplementary Fig. 1b) indicated that the particle is globular or globoid with only a small degree of flexibility, in agreement with tight packing of the Hr-like folds.

SAXS data can also be assessed in real space using the pair distance distribution function, $P(r)$, which is obtained by indirect Fourier transformation of $I(q)$ (Supplementary Fig. 1c). This analysis gave a maximum distance (d_{max}) of 98 Å, in agreement with the longest predicted axis

132 of 96.5 Å in the AlphaFold2 model. The protein envelope calculated from raw scattering data
133 using DAMMIN software[19] is shown in Fig. 2d, overlaid with a refined AlphaFold2 model. The
134 χ^2 value of the fit between model and envelope was 1.075, or 1.008 for the model to the
135 scattering data using CRYSOL analysis (Supplementary Data 1). From this we can conclude
136 that the AlphaFold2 structure is representative of the solution structure of BTSL2-N as
137 determined by SAXS.
138

139 **The Hr-like domains of BTSL2 and BTS bind diiron centres, except for H2 in BTSL2**

140 To determine the type and number of metal cofactors in the N-terminal part of BTSL2 and
141 BTS, the purified proteins were analysed by Inductively Coupled Plasma – Mass Spectrometry
142 (ICP-MS) followed by quantitative assays to determine the molar ratio of iron per polypeptide.
143 The MBP domain was not removed to maximize protein yield for these and subsequent
144 analyses (Fig. 3a-b). For BTS-N, addition of β-mercaptoethanol or glutathione to all buffers
145 was required to prevent precipitation. ICP-MS for a range of transition metals showed that iron
146 was approximately nine times more abundant than zinc or manganese associated with purified
147 MBP-BTS-N, and three times more abundant in purified MBP-BTSL2-N (Supplementary Table
148 2). Using sulfur to estimate the protein concentration, the iron-to-protein ratio was 2.2 ± 0.1 for
149 BTS and 3.0 ± 0.05 for BTSL2. These numbers are thought to be an underestimation,
150 particularly for BTS, because the sample likely contained residual glutathione.

151 Quantitative analysis of iron using a colorimetric reagent and the Bradford assay for protein
152 showed that MBP-BTSL2-N contained 3.99 ± 0.16 iron atoms per polypeptide (Fig. 3c), close
153 to the expected ratio of 4 based on the two predicted diiron binding sites in H1 and H3 (Fig.
154 1a). The as-isolated protein was yellow in colour with absorbance around 350 nm (Fig. 3d-e),
155 which is typical of diiron proteins.

156 To confirm the location of the iron-binding sites in BTSL2-N, we substituted glutamate (E) in
157 the centre of the two H-HxxxE-H-HxxxE motifs with alanine (A) by site-directed mutagenesis.
158 This Glu residue bridges the two iron atoms and E-to-A substitution is known to completely
159 abolish iron binding at hemerythrin sites[11,20]. The E98A substituted protein was isolated with
160 approximately two iron per polypeptide, and a similar result was obtained with E664A (Fig. 3a,
161 c). The single variant proteins were greyish in colour (Fig. 3d) and had lost most of the
162 absorbance in the 350 nm region (approximately 8000 M^{-1} cm^{-1}, Fig. 3e). Combining E98A and
163 E664A decreased the amount of iron associated with BTSL2-N below the detection limit of the
164 colorimetric chelator (Fig. 3c) despite some residual absorbance (Fig. 3e).

165 Purified BTS-N contained 5.87 ± 0.26 iron atoms per polypeptide (Fig. 3c), close to the
166 expected ratio of 6 for three diiron centres, one in each Hr-like subdomain. The as-isolated

167 protein was reddish in colour giving a distinct UV-visible spectrum with features at 332 and
168 420 nm (Fig. 3d-e). These are in part reminiscent of an iron-sulfur (Fe-S) cluster, but further
169 spectroscopic analysis ruled out this possibility (see below).

170 These data, together with the structure of the N-terminus, showed that BTSL2 lacks a diiron
171 centre in the distally-located H2 motif and thus has two aligned diiron centres proximal to the
172 E3 ligase domain. BTS has a full complement of three diiron centres.
173

174 **The Hr-like iron centres react with O_2 and H_2O_2**

175 Next, we investigated whether the Hr-like domains of BTSL2 and BTS are redox-active. The
176 UV-visible spectra of BTSL2-N in Fig. 3e indicated that the diiron centres are predominantly
177 in the oxidized, diferric state in the 'as-isolated' protein. Attempts to obtain proteins with diiron
178 centres in a stable reduced state under atmospheric conditions failed, and therefore samples
179 were transferred to an anaerobic chamber where they were mixed with a small excess of
180 sodium dithionite as reductant, followed by buffer exchange on a desalting column to remove
181 dithionite.

182 To probe the reaction with O_2 and H_2O_2, reduced BTSL2-N was titrated with incremental
183 aliquots of oxidant and changes in UV-visible absorbance were monitored (Fig. 4a-b). For both
184 O_2 and H_2O_2 this resulted in recovery of the absorbance signals of the as-isolated protein.
185 Changes in the circular dichroism (CD) spectrum showed similar behaviour (Supplementary
186 Fig. 2), indicating that BTSL2-N was completely re-oxidized without loss of iron cofactor.
187 Reduction of BTS-N resulted in a less pronounced decrease in absorbance at 320 – 400 nm
188 than for BTSL2-N. Addition of O_2 or H_2O_2 returned the absorbance signals to those of the 'as-
189 isolated' spectra (Fig. 4d-e).

190 The observed stoichiometries of oxidant to iron were ~0.2 for O_2 and ~0.5 for H_2O_2 (Fig. 4c,
191 f), close to the theoretical minima of 0.25 for O_2 and 0.5 for H_2O_2. The ratios are typical for
192 reactions of diiron centres, such as Dps mini-ferritins, bacterioferritin, ribonucleotide reductase
193 or alternative oxidase[21-24], with O_2 and H_2O_2 accepting four and two electrons, respectively. To
194 investigate whether the O_2 reaction proceeds via a H_2O_2 intermediate, we probed for H_2O_2
195 formation using the colorimetric dye Amplex Red. Samples of reduced BTSL2-N and BTS-N
196 protein containing 40 μM Fe^{2+} were mixed with air-saturated Amplex Red assay reagents.
197 Following reaction with 20 μM O_2, the theoretical maximum production of H_2O_2 would be 20
198 μM, assuming that all H_2O_2 formed reacted with the Amplex Red reagent. For BTSL2-N and
199 BTS-N, 24.3 and 15.6 μM H_2O_2 were detected, respectively. We also tested if glutathione could
200 reduce the diiron centres in place of dithionite. A physiological concentration of glutathione (3

mM) was mixed with anaerobic BTSL2-N, and we observed reduction of the protein, albeit at a very slow rate (Supplementary Fig. 3).

Because the stoichiometry for the reaction with O_2 was somewhat lower than expected, we investigated the possibility that the diiron centres in BTSL2-N and BTS-N were not fully reduced in the presence of excess dithionite, resulting in a proportion of semi-reduced, paramagnetic centres. Electron Paramagnetic Resonance (EPR) spectroscopy of the as-isolated proteins showed a prominent signal at g = 4.3, which was essentially absent from the spectra of the reduced proteins (Fig. 5a-b). The signal corresponds to mononuclear Fe^{3+} but represented less than 1% of the total iron in the samples (see quantification described in Materials and Methods). Both BTSL2-N and BTS-N proteins also have an anisotropic EPR signal with g-values in the ≈1.9 area, which can be attributed to a mixed-valent Fe^{2+}/Fe^{3+} centre with a μ-oxo bridging ligand rather than a μ-hydroxo-bridged species, which typically has higher g-values[25]. Again, quantification indicated that this species represented less than 1% of the total iron. Titrations of oxidised protein with dithionite did not significantly increase the amplitude of the mixed valent signals, with only a moderate increase of the signal in BTSL2-N and no change in BTS-N (Supplementary Fig. 4a-b). Interestingly, the mixed valent signal was broader and diminished in the E98A variant of BTSL2-N, associated with the H3 diiron centre that remained (Supplementary Fig. 4c).

The overall lack of signal for the majority of the iron is consistent with the expectation that the fully oxidized diiron centres are EPR silent due to antiferromagnetic coupling of the two S = 5/2 Fe^{3+} ions, which are reduced without accessing the mixed valence Fe^{2+}/Fe^{3+} form. For BTS-N, there was no specific signal in the EPR spectrum of the reduced protein with g-values typical of Fe-S clusters[26]. CD spectra of BTS/L proteins were also not consistent with those of known Fe-S proteins[27-29].

Upon re-exposure to O_2, the g = 4.3 mononuclear iron signal returned to an intensity similar to that of the as-isolated proteins (Fig. 5). By contrast, exposure to H_2O_2 resulted in a signal of much lower intensity. The mixed-valent signal was not responsive to oxidant within the timescale of observation, suggesting that this is not a physiologically relevant species. A small EPR signal at g ≈ 2 had features consistent with protein-based peroxyl radicals and was seen inconsistently among some samples; a spectrum of this signal in BTSL2-N is reported with a narrow field range in Supplementary Fig. 5.

In summary, the data demonstrated that the Hr-like domains of BTSL2 and BTS contain diiron centres that are redox-active with both O_2 and H_2O_2.

236 **Iron binding to the Hr-like domains of BTSL2 and BTS is reversible in the reduced state**

237 For BTS/L proteins to function as iron sensors, it is expected that they bind iron dynamically.
238 However, iron remained bound to the Hr-like domains of BTSL2 and BTS under the conditions
239 used for purification (Fig. 3) and following reduction and re-oxidation (Fig. 4). Therefore, we
240 tested if iron chelators can compete with, and extract iron from, BTSL2-N and BTS-N. Iron
241 release was followed in real time using colorimetric iron chelators such as Ferene[30]. The as-
242 isolated, predominantly oxidized form of BTSL2-N displayed a slow but steady rate of
243 approximately 20% iron release per hour when the protein was purified with β-
244 mercaptoethanol in the buffers, or virtually no iron release without β-mercaptoethanol (Fig.
245 6a). However, if iron was released in the ferric form, it would not have been detected because
246 Ferene specifically binds Fe^{2+}. To investigate this possibility, we mixed β-mercaptoethanol-
247 free BTSL2-N with the ferric iron chelator ethylenediaminetetraacetic acid (EDTA) and saw no
248 change in the protein's CD spectrum after 1 h (Supplementary Fig. 6). Thus, we conclude that,
249 in their oxidized, Fe^{3+} form, the diiron sites are not labile.

250 Following reduction of BTSL2-N with dithionite and removal of excess reductant, exposure to
251 Ferene resulted in release of ~50% of the iron in the first few seconds, and then another 5%
252 more slowly over an hour. For BTS-N, the oxidized sample released ~15% iron over an hour,
253 whereas the reduced protein rapidly released ~30% and then another 20% at a much slower
254 rate (Fig. 6d). Equivalent experiments with reduced BTSL2-N using two other colorimetric iron
255 chelators, dipyridyl or ferrozine[31,32], gave similar results in terms of the percentage of iron
256 released and the kinetics (Supplementary Fig. 7). This demonstrated that the Fe^{2+}-protein
257 dissociation rate, rather than Fe^{2+}-chelator association rate, was measured in these
258 experiments.

259 For both BTSL2-N and BTS-N, not all of the iron was released, indicating that iron in one or
260 more of the diiron centres is not labile, even when reduced. To further investigate this for
261 BTSL2-N, iron release experiments were repeated with the E98A and E664A variant proteins.
262 Reduced E98A BTSL2-N, in which the H3 diiron centre remains intact, released ~85% of the
263 iron in the first rapid phase but did not exhibit the slower release phase observed in the wild-
264 type form (Fig. 6b). The reduced E664A protein, in which the H1 diiron centre remains intact,
265 released ~45% of its iron, mostly in the rapid first phase (Fig. 6c). Combining these values
266 equates to a release of 67% iron, which is relatively close to the 60% released from BTSL2-N
267 with both diiron centres. The data indicate that the H3 diiron centre is more labile, releasing
268 up to both irons. The H1 diiron centre is also labile but releases one iron only. In addition,
269 kinetics of both single variants appeared altered relative to the wild-type protein, suggesting
270 that the iron status of one diiron centre affects the other.

271 To investigate whether iron binding is reversible, we tested for re-association of iron after the
272 removal of the labile iron atoms. The experimental procedure, as outlined in Fig. 7a, was
273 followed using CD spectroscopy because only protein-bound iron contributes to the spectrum.
274 Under anaerobic conditions, a defined amount of Ferene was added to reduced BTSL2-N to
275 remove 40% of the Fe^{2+} (i.e. less than the proportion removed in the fast phase when excess
276 chelator was added, see Fig. 6a). To verify that the iron was indeed removed, half the sample
277 was desalted and oxidized, yielding a CD spectrum with a commensurate decrease in the CD
278 signal at 350 nm (Fig. 7b, blue trace). To the other half of the sample, kept under anaerobic
279 conditions, a 3-fold excess of Fe^{2+} in the form of ferrous ammonium sulfate was added followed
280 by a desalting step to remove unbound iron and iron-chelator complexes. After exposure to O_2,
281 the resulting CD spectrum was identical to that of the as-isolated protein (Fig. 7b, pink trace),
282 indicating full occupancy of the diiron centres and successful re-association of the iron that had
283 been removed. Overall, these data demonstrate that, in a reducing environment, iron binding
284 to BTS/Ls is reversible. By contrast, in an oxidizing environment, iron remained tightly bound.

285

286 **Impaired iron binding and redox activity in the H1 subdomain affects the function of**
287 **BTS in vivo**

288 We previously identified a mutation in the N-terminal domain of BTS that causes the plant to
289 hyper-accumulate iron[33]. The in-frame deletion removes 5 amino acid residues from the first
290 Hr-like sequence close to two iron-binding ligands (Fig. 8a). The phenotypic consequences of
291 the mutation, called *dgl*, have been studied extensively in pea (*Pisum sativum*) since it was
292 identified several decades ago[34,35]. The transcript levels of two iron uptake genes, *Ferric*
293 *Reduction Oxidase 1* (*PsFRO1*) and *Iron-Regulated Transporter 1* (*PsIRT1*), were shown to
294 be highly induced in *dgl* roots and did not decrease in response to addition of iron[36]. By
295 contrast in wild-type plants, the levels of these transcripts were below the limit of detection
296 under normal (+Fe) conditions. *FRO* and *IRT1* are downstream of the transcription factors
297 ILR3/bHLH105 and bHLH115, which have recently been confirmed as ubiquitination
298 substrates of BTS in Arabidopsis[2,5,9]. The Arabidopsis and pea *BTS* genes are functional
299 orthologs[33] and thus it can be deduced that the E3 ligase activity is diminished in the BTS^{dgl}
300 protein, upregulating the downstream signalling pathway and iron uptake genes.

301 To investigate whether iron binding and/or redox activity is affected in the BTS^{dgl} protein, the
302 equivalent five amino acids were deleted from the Arabidopsis sequence in the BTS-N
303 expression construct. The *dgl* variant protein was expressed and purified using the same
304 conditions as for BTS-N (Fig. 8b). Although the yield of BTS^{dgl}-N was ~7-fold lower than for
305 the wild-type protein, the mutant variant was equally stable through subsequent analyses. Iron

306 quantification showed that the *dgl* variant bound 4 ± 0.18 iron per polypeptide, correlating with
307 the lower molar absorptivity in the 300 – 500 nm range of the as-isolated protein compared to
308 BTS-N (Fig. 8c, solid lines). The data indicated that the recombinant *dgl* protein lacked the
309 diiron centre in the H1 subdomain.

310 Upon reduction with dithionite, the BTS^{dgl}-N and BTS-N wild-type proteins showed similar UV-
311 visible spectra (Fig. 8c, dotted lines), apart from the absorbance feature at 425 nm which was
312 more pronounced in the *dgl* variant protein. Upon reoxidation by exposure to air, the UV-visible
313 spectrum of wild-type BTS reverted to the as-isolated spectrum. However, for BTS^{dgl}-N, only
314 half the original absorptivity was recovered, even after longer incubation (50 min). Comparison
315 of the EPR spectra showed that the minority mixed-valent signal was lacking in BTS^{dgl}
316 (Supplementary Fig. 8), indicating that this signal arises from or is dependent on the H1 diiron
317 centre. Thus, impaired iron binding and reoxidation of BTS^{dgl} in vitro are correlated with
318 compromised functionality of the E3 ubiquitin ligase in vivo.

319

320 **DISCUSSION**

321 Physiological and genetic studies firmly point to BTS/L proteins as the iron sensors that switch
322 off the iron deficiency response in plants, but biochemical evidence has been lacking. Our in-
323 depth study of the iron-binding and redox properties of the N-terminal Hr-like domain leads us
324 to propose a mechanism by which BTS/L proteins are activated in response to increasing iron
325 levels and oxidative stress (Fig. 9). The expression of BTS/L is induced by iron deficiency, so
326 when the proteins are initially produced it is likely that the iron-binding sites are only partially
327 occupied. Partial iron binding could be important for maintaining the protein in a folded, but
328 inactive, state. As iron levels increase, the diiron centres fill. As and when the cellular
329 environment experiences oxidative stress conditions, rapid oxidation of the diiron centres
330 decreases the lability of the iron and shifts the protein into its active conformation, which is
331 now able to ubiquitinate its cognate transcription factors, shutting down iron uptake.

332 The model makes certain assumptions and also leaves several open questions, to be tested
333 in future experiments. First, the proposed mechanism would allow distinction between iron-
334 induced oxidative stress and oxidative stress from other sources. We suggest that iron binding
335 to BTS/L (without oxidation) is insufficient to trigger activation. As multicellular organisms,
336 plants have cells that experience relatively high intracellular iron concentrations, for example
337 vascular tissues involved in iron transport. Their role is to pass the iron on to neighbouring
338 cells, and this flux should not be suppressed too easily by BTS/L activation. Having said that,
339 unicellular algae also have BTS proteins, perhaps to maximize iron flow to chloroplasts which
340 are a large sink of iron in photosynthetic cells.

341 Second, we speculate that the E3 ligase is activated through conformational changes that
342 enable binding of the cognate E2 partner and/or substrate proteins, although other
343 mechanisms are also possible. The observation that expression of BTS lacking the N-terminal
344 triple Hr-like domain is more abundant and more active in planta[5] suggests that this form is
345 constitutively active. Possibly, the mostly rigid triple Hr-like domain, which is connected by a
346 flexible linker to the E3 ligase domain, could have an auto-inhibitory function through large
347 conformational changes. To investigate this, expression and purification of sufficient amounts
348 of the full-length proteins is needed and efforts towards this are currently ongoing.

349 Interesting parallels between mammalian FBXL5 and plant BTS/L proteins are the use of diiron
350 centres in Hr-like folds for sensing iron, linked to ubiquitin ligase activation. However, our
351 characterization of the BTS/L Hr-like domains also revealed fundamental differences, which
352 are likely to impact on the mechanism of iron sensing. Phylogenetic analysis (Fig. 1a) showed
353 the invariant presence of three Hr-like subdomains in BTS/L, intertwined in a rigid triple domain
354 (SAXS data, Fig. 2 and Supplementary Fig. 1). Several lines of evidence indicate that the three
355 Hr-like subdomains of BTS/L do not function independently of each other. Most strikingly, the
356 remaining intact diiron centres (H2 and H3) of the *dgl* variant BTS protein exhibited incomplete
357 reduction and re-oxidation behaviour (Fig. 8), demonstrating that the absence of the H1 diiron
358 centre affects the properties of the other two. This could be an effect on redox activity, or on
359 iron binding affinity, or both. Inter-dependency of, or cooperativity between, the Hr motifs is
360 consistent with the spectra (colour) of the two BTSL2 variants E98A and E664A (Fig. 3), which
361 each lack one of the two diiron centres of the wild-type protein. As isolated, these variants
362 exhibited absorption properties that were similar to each other but quite different form the wild-
363 type protein, in that they lacked the absorbance shoulder at 350 nm. Independent behaviour
364 would be expected to result in spectra similar to that of wild-type protein but of weaker intensity.
365 Different behaviour was also noted in iron-release experiments, where the slow phase of
366 release was much reduced in both variants (Fig. 6). Thus, while further data on the
367 transduction of the signal from the Hr-like domain to the E3 ligase domain are needed, it is
368 highly likely that the three Hr-like motifs function in a coordinated and inter-dependent manner
369 that affects their redox properties.

370 Aside from the higher order architecture, the properties of the diiron centres appear similar in
371 BTS/L proteins and FBXL5: The UV-visible spectra of BTSL2 (Fig. 3d) and FBXL5[37,38] are
372 comparable and both proteins have a relatively fast autoxidation rate (Fig. 4 and Refs. [39-41]).
373 AlphaFold models of BTS/Ls compared with the crystal structure of FBXL5[37] suggest a similar
374 coordination geometry of the diiron centres. The ligand binding is asymmetric, with one iron
375 hexa- and the other iron penta-coordinated, which is likely to cause their differential lability as
376 observed here for BTS/L proteins (Fig. 6b-c).

377 Iron binding stabilizes the FBXL5 protein[10,11] and recent data showed that BTS from soybean
378 is stabilized by iron when transiently expressed in tobacco (*N. benthamiana*) leaves[42].
379 However, previously a destabilizing effect by iron was reported when Arabidopsis BTS was
380 expressed in a wheat-germ expression system[5]. We have repeated this experiment and found
381 that iron inhibits the transcription or translation in this cell-free system but not the stability of
382 the protein (Supplementary Fig. 9a). Attempts to remove all iron from oxidized BTSL2-N
383 gradually by increasing the temperature in the presence of an iron chelator resulted in
384 precipitation of the protein (Supplementary Fig. 9b). From these experiments and our iron
385 binding studies (Fig. 6 and 7), we conclude that the BTS/L N-terminus with partially occupied
386 diiron centres is folded, and that iron is required for stability of the protein.

387 The need for a thiolate reductant such as β-mercaptoethanol or glutathione to purify stable
388 BTS-N suggests that glutathione plays a physiological role in the iron sensing mechanism.
389 Decreased glutathione levels as a consequence of mutations in the biosynthesis pathway
390 render Arabidopsis seedlings more sensitive to iron deficiency. In those mutants, key genes
391 required for iron uptake, including *IRT1* and *FRO2*, were expressed at much lower levels than
392 in wild-type plants[43]. It is tempting to speculate that in these mutants the redox equilibrium of
393 the BTS/L proteins is shifted more towards the oxidized form (Fig. 9), leading to increased
394 ubiquitination followed by degradation of the transcription factors of the iron deficiency
395 response.

396 The iron-binding and redox properties of the unique triple Hr-like domain of BTS/L proteins
397 shed the first light on the sensing mechanism of these important negative regulators of the
398 iron deficiency response in plants. This will facilitate mutant studies to probe the mechanism
399 in planta, and to potentially modify the system for increasing iron uptake in specific plant
400 tissues for human nutrition, known as biofortification.

401

402 **METHODS**

403 **Protein expression and purification**

404 Coding sequences of the N-terminal domains of *BTS* (AT3G18290) and *BTSL2* (AT1G18910)
405 were amplified from *Arabidopsis thaliana* cDNA using the primers listed in Supplementary
406 Table 3 and cloned into the pMAL-c5x vector (New England Biolabs). The variant BTSL2 and
407 BTS proteins were made by site-direct mutagenesis using the listed primers and either the
408 QuikChange Lightning Site-Directed Mutagenesis Kit (Agilent) or the QS Site Directed
409 Mutagenesis Kit (New England Biolabs) according to the supplier's manual. For the BTS^{dgl}
410 variant, the linearized plasmid excluding the 15-nucleotide deletion was blunt-end ligated.

411 The resulting plasmids were used to transform BL21-DE3 Rosetta-pISC *E. coli* cells[44]. The
412 transformed cells were cultured in 4 L Terrific broth containing 0.02% (v/v) glucose at 37 °C to
413 an OD_{600} of 1.1-1.2. Flasks were incubated in an ice bath for 15 min, then induced with 100
414 μM IPTG, 0.05% (v/v) DMSO and 50 μM ferric ammonium citrate o/n at 16 °C. Cells were
415 harvested and resuspended in 100 mM Tris-HCl, 150 mM NaCl, 20 mM β-mercaptoethanol,
416 pH 8.0 with cOmplete EDTA-free protease inhibitor (1 tablet/ 50 mL). Cells were disrupted
417 using an ultrasonics processor (Vibra-Cell VCX 750, Sonics) during 60 cycles of 2 s on, 8 s
418 off at 40% power while samples were cooled in ice water. The resulting lysate was centrifuged
419 at 20,000 × g for 30 min at 4 °C. The soluble fraction was loaded onto a 5 mL Strep-Tactin XT
420 column (IBA Lifesciences) and washed with 100 mM Tris-HCl, 150 mM NaCl, 20 mM β-
421 mercaptoethanol, pH 8.0. Protein was eluted with 100 mM Tris-HCl, 150 mM NaCl, 20 mM β-
422 mercaptoethanol, 50 mM D-biotin, pH 8.0. Removing β-mercaptoethanol from purification
423 buffers after sonication for MBP-BTSL2-N had no effect on the final Fe:protein ratios. Proteins
424 were concentrated using a spin concentrator (MWCO 30 kDa, Pierce). For SAXS experiments,
425 affinity-purified MBP-BTSL2-N-Strep was cleaved using Factor Xa protease (NEB, product no.
426 P9010L) at a concentration of ~2.8 ng mL^{-1} for 24 h at 4 °C. Cleaved protein was buffer-
427 exchanged into 10 mM MES, 15 mM NaCl, pH 6.5 using a spin concentrator (MWCO 30 kDa,
428 Pierce) and BTSL2-N was isolated via size-exclusion chromatography using an S200 26/60
429 Sephadex column (Cytiva). The identity of the purified BTS-N and BTS^{dgl}-N variant proteins
430 was confirmed by LC-MS of the intact proteins.

431 **Quantification of iron and other metals**

432 Protein samples were buffer exchanged into 10 mM Tris-HCl, pH 8.0 and analysed using
433 inductively coupled plasma – mass spectrometry (ICP-MS; Triple Quadrupole iCAP-TQ from
434 ThermoFisher). Iron in protein samples was also quantified using the colorimetric reagent 3-
435 (2-pyridyl)-5,6-bis(2-(5-furyl sulfonic acid)-1,2,4-triazine, also called Ferene[30]. Protein samples
436 were quantified using the Bradford assay (Protein Assay Dye Reagent, BioRad).

437 **Small-angle X-ray scattering**

438 SAXS data were collected at Diamond Light Source (DLS; Oxfordshire, UK) on beamline 21
439 in a standard SEC-SAXS experiment. Samples at 1 to 5 mg mL^{-1} were applied to a Superdex
440 200 increase column (Cytiva, Amersham, UK) and run at a flow rate of 0.075 mL min^{-1} in 10
441 mM MES, 15 mM NaCl, pH 6.5. Data were recorded at a wavelength of 0.9464 Å using an
442 EigerX 4M detector (Dectris, Baden-Daettwil, Switzerland). Measurements were performed at
443 15 °C within the q range 0.0045 – 0.34 $Å^{-1}$ ($q = 4\pi\sin\theta/\lambda$; 2θ is the scattering angle, λ is the
444 wavelength) with a sample-to-detector distance of 3.72 m. Data were normalized for water
445 scattering on an absolute scale. From the SEC-SAXS run of the 5 mg mL^{-1} protein sample
446 frames 372-375 were selected, merged and solvent subtracted for data analysis using ScÅtter

447 (https://sibyls.als.lbl.gov/scatter/), IV.d and ATSAS 3.2.1[45]. Calculation of R_g and forward
448 scattering $I(0)$ was performed by Guinier approximation after removing the first 30 data points,
449 The maximum dimension of the particle d_{max} and the *P(r)* function were estimated using the
450 program GNOM[46]. Ab initio envelope models were computed using DAMMIN[19] and overlaid
451 with an AlphaFold2 model[47,48] that was refined against the scattering data using SASREF[49].
452 The bound iron centres were populated manually via structure superposition with existing PDB
453 entry 2AVK and model editing in the COOT software[50]. Experimental data and models were
454 prepared using IUCr guidelines[51,52], as summarized in Supplementary Data 1.

455 **Titrations with O_2 or H_2O_2**

456 The MBP-fusion proteins of the BTSL2 and BTS N-terminal domains were stable at room
457 temperature in a glovebox over a 12 h period, during which redox studies could be performed
458 in an anaerobic environment. Buffer solutions were sparged with N_2 gas for 1 h before being
459 left to equilibrate in an anaerobic (<2 ppm O_2) chamber overnight. Protein aliquots were
460 thawed inside the chamber. Gas-tight quartz cuvettes with a 10 mm pathlength (Starna Cells,
461 UK) were used to transfer the protein in and out of the chamber for measurement. Sodium
462 dithionite was prepared in anaerobic buffer and its concentration was determined using an
463 extinction coefficient, ε_{315} = 8000 M^{-1} cm^{-1} (Ref[53]). A threefold excess of dithionite was added
464 relative to the protein's iron content and incubated anaerobically. Reduction of the protein was
465 confirmed using circular dichroism measurements made on a Jasco J-810 CD
466 spectropolarimeter to monitor loss of the protein's absorbance peak due to Fe^{3+} at ≈350 nm.
467 Protein was then buffer exchanged on a PD10 desalting column (Cytiva). Aliquots of protein
468 were then titrated with known volumes of H_2O_2 prepared in anaerobic buffer or with aerobic
469 buffer. After each addition of oxidant, a minimum of three minutes elapsed before recording
470 the sample's absorbance or CD spectrum. Absorbance spectra were recorded using a Jasco
471 V550 spectrophotometer.

472 **Electron Paramagnetic Resonance**

473 Proteins were degassed, reduced and desalted as above. Proteins were mixed within an
474 anaerobic chamber with the appropriate volume of a supersaturated O_2 solution (prepared by
475 bubbling pure O_2 through 100 mM Tris-HCl, 150 mM NaCl, pH 8.0 in a suba-sealed volumetric
476 flask), estimated to be 1.2 mM, or a 1.2 mM H_2O_2 solution, and then transferred into EPR
477 tubes. For titrations with sodium dithionite, aliquots of protein were mixed in an anaerobic
478 chamber with the appropriate volume of a 1.5 mM dithionite solution in plastic cannulae and
479 ejected into EPR tubes. Sealed tubes were removed from the chamber and frozen after the
480 stated reaction times by dropping into methanol cooled in dry ice. Spectra were recorded on
481 a Bruker E500 (X band) EPR spectrometer at 10 K equipped with an Oxford Instruments liquid-
482 helium system. Quantification of the paramagnetic species was done by comparison of second

483 integrals of the species' pure line shape EPR signals, obtained by the spectra subtraction with
484 variable coefficient procedure[54], with those of the two concentration standards used. For
485 quantification, the microwave power saturation dependences of all signals were measured
486 and taken into account (Supplementary Fig. 10). The mixed valent (Fe^{2+}/Fe^{3+}) species was
487 quantified using a 1 mM Cu^{2+}[EDTA] concentration standard, and the mono-nuclear ferric
488 signals using a 35 μM ferric iron binding protein from *Neisseria gonorrhoeae*.

489 **Amplex Red assay**

490 H_2O_2 release from reduced BTS/L proteins was detected using an Amplex Red kit (Thermo
491 Fisher) according to the manufacturer's instructions. Briefly, a 200 μL aliquot of freshly
492 prepared aerobic Amplex Red reaction mixture was mixed with a 200 μL anaerobic aliquot of
493 reduced BTS/L protein, diluted so that the protein-bound iron concentration was 40 μM. The
494 absorbance at 571 nm was used to quantify H_2O_2 based on a calibration curve using 0-37.5
495 μM H_2O_2.

496 **Iron chelator competition assays**

497 For 'as-isolated' measurements, proteins were thawed in an anaerobic glovebox. For the
498 reduced samples, proteins were treated with dithionite and desalted as described above. Each
499 protein sample was then diluted in a sealed cuvette and single wavelength time courses were
500 recorded using a Jasco V550 spectrophotometer after mixing with colorimetric chelators.
501 Monitored wavelengths were 592, 525, and 562 nm for Ferene, 4,4' dipyridyl and ferrozine,
502 respectively. The final concentration of iron in each assay was 75 μM, and that for each
503 chelator was 1 mM. The percentage iron released was measured relative to calibration curves
504 prepared for each chelator mixed with 0, 10, 25, 50 and 75 μM Mohr's salt anaerobically
505 prepared in 100 mM Tris-HCl, 150 mM NaCl, pH 8.0.

506 **Reconstitution of BTSL2**

507 BTSL2-N (86 μM, 3.8 Fe per protein) was reduced and desalted as above. Ferene sufficient
508 to remove 40% of the iron within the protein was added, and iron removal confirmed using
509 absorbance at 593 nm. Ferrous ammonium sulfate in 3-fold excess over freshly de-occupied
510 iron binding sites was added to the protein under anaerobic conditions, after which the sample
511 was again desalted. The protein was exposed to air for 10 min in an open Eppendorf with
512 gentle mixing. UV-visible absorbance and CD spectra were recorded after each manipulation.
513 Each CD spectrum represents the average of four measurements to improve signal:noise
514 ratio; for the final sample (air exposed, reconstituted BTSL2) the spectrum was the average
515 of sixteen measurements.

516

517

REFERENCES

1. Rodriguez-Celma, J., Chou, H., Kobayashi, T., Long, T.A. & Balk, J. Hemerythrin E3 ubiquitin ligases as negative regulators of iron homeostasis in plants. *Front. Plant. Sci.* **10**, 98 (2019).
2. Hindt, M.N. et al. BRUTUS and its paralogs, BTS LIKE1 and BTS LIKE2, encode important negative regulators of the iron deficiency response in *Arabidopsis thaliana*. *Metallomics* **9**, 876-890 (2017).
3. Rodriguez-Celma, J. et al. Arabidopsis BRUTUS-LIKE E3 ligases negatively regulate iron uptake by targeting transcription factor FIT for recycling. *Proc. Natl. Acad. Sci.* **116**, 17584-17591 (2019).
4. Kobayashi, T. et al. Iron-binding haemerythrin RING ubiquitin ligases regulate plant iron responses and accumulation. *Nat. Commun.* **4**, 2792 (2013).
5. Selote, D., Samira, R., Matthiadis, A., Gillikin, J.W. & Long, T.A. Iron-binding E3 ligase mediates iron response in plants by targeting basic helix-loop-helix transcription factors. *Plant Physiol.* **167**, 273-86 (2015).
6. Tzafrir, I. et al. Identification of genes required for embryo development in Arabidopsis. *Plant Physiol.* **135**, 1206-1220 (2004).
7. Alvarez-Carreno, C., Alva, V., Becerra, A. & Lazcano, A. Structure, function and evolution of the hemerythrin-like domain superfamily. *Protein Sci.* **27**, 848-860 (2018).
8. Lichtblau, D.M. et al. The iron deficiency-regulated small protein effector FEP3/IRON MAN1 modulates interaction of BRUTUS-LIKE1 with bHLH subgroup IVc and POPEYE transcription factors. *Front. Plant. Sci.* **13**, 930049 (2022).
9. Li, Y. et al. IRON MAN interacts with BRUTUS to maintain iron homeostasis in Arabidopsis. *Proc. Natl. Acad. Sci.* **118**(2021).
10. Vashisht, A.A. et al. Control of iron homeostasis by an iron-regulated ubiquitin ligase. *Science* **326**, 718-21 (2009).
11. Salahudeen, A.A. et al. An E3 ligase possessing an iron-responsive hemerythrin domain is a regulator of iron homeostasis. *Science* **326**, 722-6 (2009).
12. Wang, H. et al. FBXL5 regulates IRP2 stability in iron homeostasis via an oxygen-responsive [2Fe2S] cluster. *Mol. Cell.* **78**, 31-41 (2020).
13. Urzica, E.I. et al. Systems and trans-system level analysis identifies conserved iron deficiency responses in the plant lineage. *Plant Cell* **24**, 3921-3948 (2012).
14. Matthiadis, A. & Long, T.A. Further insight into BRUTUS domain composition and functionality. *Plant Signal Behav.* **11**, e1204508 (2016).
15. Davidi, L. et al. Pumping iron: A multi-omics analysis of two extremophilic algae reveals iron economy management. *Proc. Natl. Acad. Sci.* **120**, e2305495120 (2023).
16. Gommes, C.J., Jaksch, S. & Frielinghaus, H. Small-angle scattering for beginners. *J. Appl. Crystallogr.* **54**, 1832-1843 (2021).
17. Hajizadeh, N.R., Franke, D., Jeffries, C.M. & Svergun, D.I. Consensus Bayesian assessment of protein molecular mass from solution X-ray scattering data. *Sci. Rep.* **8**, 7204 (2018).
18. Franke, D. & Svergun, D.I. DAMMIF, a program for rapid ab-initio shape determination in small-angle scattering. *J. Appl. Crystallogr.* **42**, 342-346 (2009).
19. Lombardi, A. et al. Retrostructural analysis of metalloproteins: application to the design of a minimal model for diiron proteins. *Proc. Natl. Acad. Sci.* **97**, 6298-6305 (2000).
20. Pullin, J. et al. Iron oxidation in *Escherichia coli* bacterioferritin ferroxidase centre, a site designed to react rapidly with H_2O_2 but slowly with O_2. *Angew. Chem. Int. Ed.* **133**, 8361-8369 (2021).
21. Elgren, T.E. et al. Electron transfer associated with oxygen activation in the B2 protein of ribonucleotide reductase from *Escherichia coli*. *J. Biol. Chem.* **266**, 19265-19268 (1991).
22. Zhao, G. et al. Iron and hydrogen peroxide detoxification properties of DNA-binding protein from starved cells. A ferritin-like DNA-binding protein of *Escherichia coli*. *J. Biol. Chem.* **277**, 27689-27696 (2002).

23. Yamasaki, S. et al. Weak O_2 binding and strong H_2O_2 binding at the non-heme diiron center of trypanosome alternative oxidase. *Biochim. Biophys. Acta, Bioenerg.* **1862**, 148356 (2021).
24. Davydov, R.M., Ménage, S., Fontecave, M., Gräslund, A. & Ehrenberg, A. Mixed-valent μ-oxo-bridged diiron complexes produced by radiolytic reduction at 77 K studied by EPR. *J. Biol. Inorg. Chem.* **2**, 242-255 (1997).
25. Hagen, W.R. EPR spectroscopy of iron—sulfur proteins. in *Advances in inorganic chemistry*, Vol. 38 165-222 (Academic Press, 1992).
26. Stephens, P.J. et al. Circular dichroism and magnetic circular dichroism of iron-sulfur proteins. *Biochemistry* **17**, 4770-4778 (1978).
27. Pellicer Martinez, M.T. et al. Sensing iron availability via the fragile [4Fe-4S] cluster of the bacterial transcriptional repressor RirA. *Chem. Sci.* **8**, 8451-8463 (2017).
28. Guo, Z. et al. Modulation of MagR magnetic properties via iron-sulfur cluster binding. *Sci Rep* **11**, 23941 (2021).
29. Hennessy, D.J., Reid, G.R., Smith, F.E. & Thompson, S.L. Ferene — a new spectrophotometric reagent for iron. *Can. J. Chem.* **62**, 721-724 (1984).
30. Irving, H. & Mellor, D.H. The stability of metal complexes of 1,10-phenanthroline and its analogues. Part I. 1,10-Phenanthroline and 2,2'-bipyridyl. *J. Chem. Soc.* **0**, 5222-5237 (1962).
31. Carter, P. Spectrophotometric determination of serum iron at the submicrogram level with a new reagent (ferrozine). *Anal. Biochem.* **40**, 450-458 (1971).
32. Harrington, S.A., Franceschetti, M. & Balk, J. Genetic basis of the historical iron-accumulating *dgl* and *brz* mutants in pea. *Plant J.* **117**, 590-598 (2024).
33. Gottschalk, W. Improvement of the selection value gene *dgl* through recombination. *Pisum Newsletter* **19**, 9-11 (1987).
34. Kneen, B.E., Larue, T.A., Welch, R.M. & Weeden, N.F. Pleiotropic effects of *brz*: a mutation in *Pisum sativum* (L.) cv 'Sparkle' conditioning decreased nodulation and increased iron uptake and leaf necrosis. *Plant Physiol.* **2**, 717-722 (1990).
35. Garcia, M.J. et al. Shoot to root communication is necessary to control the expression of iron-acquisition genes in Strategy I plants. *Planta* **237**, 65-75 (2013).
36. Thompson, J.W. et al. Structural and molecular characterization of iron-sensing hemerythrin-like domain within F-box and leucine-rich repeat protein 5 (FBXL5). *J. Biol. Chem.* **287**, 7357-7365 (2012).
37. Wei, Y., Yuan, H., Xu, P. & Tan, X. Redox sensing molecular mechanism of an iron metabolism regulatory protein FBXL5. *Arch. Biochem. Biophys.* **616**, 30-39 (2017).
38. Arkosi, M., Scurtu, F., Vulpoi, A., Silaghi-Dumitrescu, R. & Kurtz, D., Jr. Copolymerization of recombinant *Phascolopsis gouldii* hemerythrin with human serum albumin for use in blood substitutes. *Artif. Cells Nanomed. Biotechnol.* **45**, 218-223 (2017).
39. Arii, H. et al. A novel diiron complex as a functional model for hemerythrin. *J. Inorg. Biochem.* **82**, 153-162 (2000).
40. Crack, J.C. et al. The di-iron protein YtfE is a nitric oxide-generating nitrite reductase involved in the management of nitrosative stress. *J. Am. Chem. Soc.* **144**, 7129-7145 (2022).
41. Ren, Z. et al. The BRUTUS iron sensor and E3 ligase facilitates soybean root nodulation by monoubiquitination of NSP1. *Nat. Plants* (2025).
42. Shanmugam, V., Wang, Y.W., Tsednee, M., Karunakaran, K. & Yeh, K.C. Glutathione plays an essential role in nitric oxide-mediated iron-deficiency signaling and iron-deficiency tolerance in Arabidopsis. *Plant J.* **84**, 464-477 (2015).
43. Grawert, T. et al. IspH protein of *Escherichia coli*: studies on iron-sulfur cluster implementation and catalysis. *J. Am. Chem. Soc.* **126**, 12847-12855 (2004).
44. Manalastas-Cantos, K. et al. ATSAS 3.0: expanded functionality and new tools for small-angle scattering data analysis. *J. Appl. Crystallogr.* **54**, 343-355 (2021).
45. Svergun, D.I. Determination of the regularization parameter in indirect-transform methods using perceptual criteria. *J. Appl. Crystallogr.* **25**, 495-503 (1992).

620 46. Jumper, J. et al. Highly accurate protein structure prediction with AlphaFold. *Nature* **596**,
621 583-589 (2021).
622 47. Skolnick, J., Gao, M., Zhou, H. & Singh, S. AlphaFold 2: why It works and its implications for
623 understanding the relationships of protein sequence, structure, and function. *J. Chem. Inf.*
624 *Model.* **61**, 4827-4831 (2021).
625 48. Petoukhov, M.V. & Svergun, D.I. Global rigid body modeling of macromolecular complexes
626 against small-angle scattering data. *Biophys. J.* **89**, 1237-1250 (2005).
627 49. Emsley, P. & Cowtan, K. Coot: model-building tools for molecular graphics. *Acta Crystallogr. D*
628 **60**, 2126-2132 (2004).
629 50. Trewhella, J. et al. 2017 publication guidelines for structural modelling of small-angle
630 scattering data from biomolecules in solution: an update. *Acta Crystallogr. D* **73**, 710-728
631 (2017).
632 51. Trewhella, J., Jeffries, C.M. & Whitten, A.E. 2023 update of template tables for reporting
633 biomolecular structural modelling of small-angle scattering data. *Acta Crystallogr. D* **79**, 122-
634 132 (2023).
635 52. Dixon, M. The acceptor specificity of flavins and flavoproteins. I. Techniques for anaerobic
636 spectrophotometry. *Biochim. Biophys. Acta, Bioenerg.* **226**, 241-258 (1971).
637 53. Svistunenko, D.A., Davies, N., Brealey, D., Singer, M. & Cooper, C.E. Mitochondrial dysfunction
638 in patients with severe sepsis: an EPR interrogation of individual respiratory chain
639 components. *Biochim Biophys Acta* **1757**, 262-272 (2006).
640 54. Dereeper, A. et al. Phylogeny.fr: robust phylogenetic analysis for the non-specialist. *Nucleic*
641 *Acids Res.* **36**, W465-9 (2008).

642

643 **Acknowledgements**

644 We thank our colleagues: Dr. Myles Cheesman for use of the CD spectrometer; Graham
645 Chilvers for ICP-MS; Jason Crack for protein mass spectrometry, technical advice and
646 discussion; Dominic Campopiano (University of Edinburgh) for providing ferric iron binding
647 protein from *Neisseria gonorrhoeae*; Mark Thornton, Mei Ying Nam and Robert Griffith
648 (summer students) for protein expression. We acknowledge Diamond Light Source for access
649 to SAXS beamline B21 under proposal MX25108 and beamline scientist Katsuaki Inoue for
650 collecting the data. This work was supported by the Biotechnology and Biological Sciences
651 Research Council, grant awards BB/N001079/1 (to J.R.C, M.F., N.E.L.B. and J.B.);
652 BB/V015095/1 (to J.P., M.F. and J.B.); BB/V014625/1 (to J.M.B. and N.E.L.B.); and
653 BB/R013578/1 for the purchase of an ICP-QQQ-MS instrument (J.B. and N.E.L.B). J.R.C.
654 received additional support from the NextGenerationEU program, award TED2021-130539A-
655 I00; and MCIN/AEI/10.13039/501100011033.

656 **Author contributions**

657 N.E.L.B. and J.B. conceived the project. J.P. carried out the majority of the experiments with
658 guidance from J.M.B. J.R.-C. and M.F. made the expression constructs. J.E.A.M. performed
659 SAXS analysis. D.A.S. supervised the EPR analysis. J.B. wrote the paper and all authors
660 reviewed, edited, and commented on the draft. N.E.L.B. and J.B. jointly supervised the project.

661 **FIGURES**

662

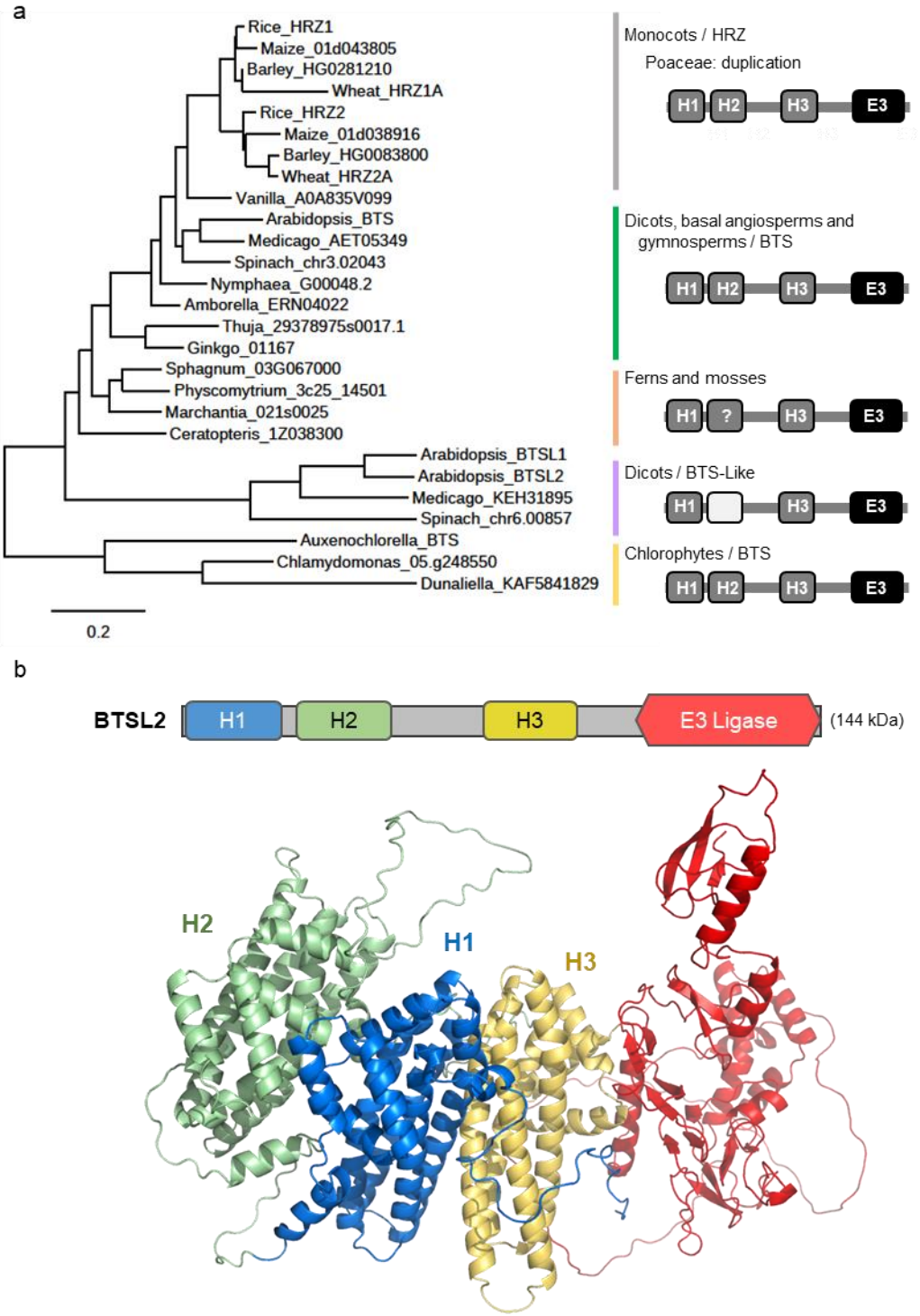

663

664 **Fig. 1 Conserved domain organisation of HRZ/BTS proteins and predicted protein fold.**

665 **a** Phylogeny of HRZ, BTS and BTS-Like (BTSL) proteins from selected organisms across the green
666 lineage (left) and their domain organisation (right). The hemerythrin (Hr)-like sequences are marked H1,
667 H2 and H3. Dark grey indicates the presence, and light grey the absence, of iron-binding ligands. The
668 question mark indicates that one of the six ligands is absent or not aligned. For full species names and

669 sequence IDs, see Supplementary Table 1. Phylogenetic analysis was performed using
670 www.phylogeny.fr[16]. The scale bar indicates the number of amino acid substitutions per site. **b**
671 AlphaFold2 model of BTSL2. The Hr-like folds are predicted to be ordered H2–H1–H3 in a tightly packed
672 configuration.
673

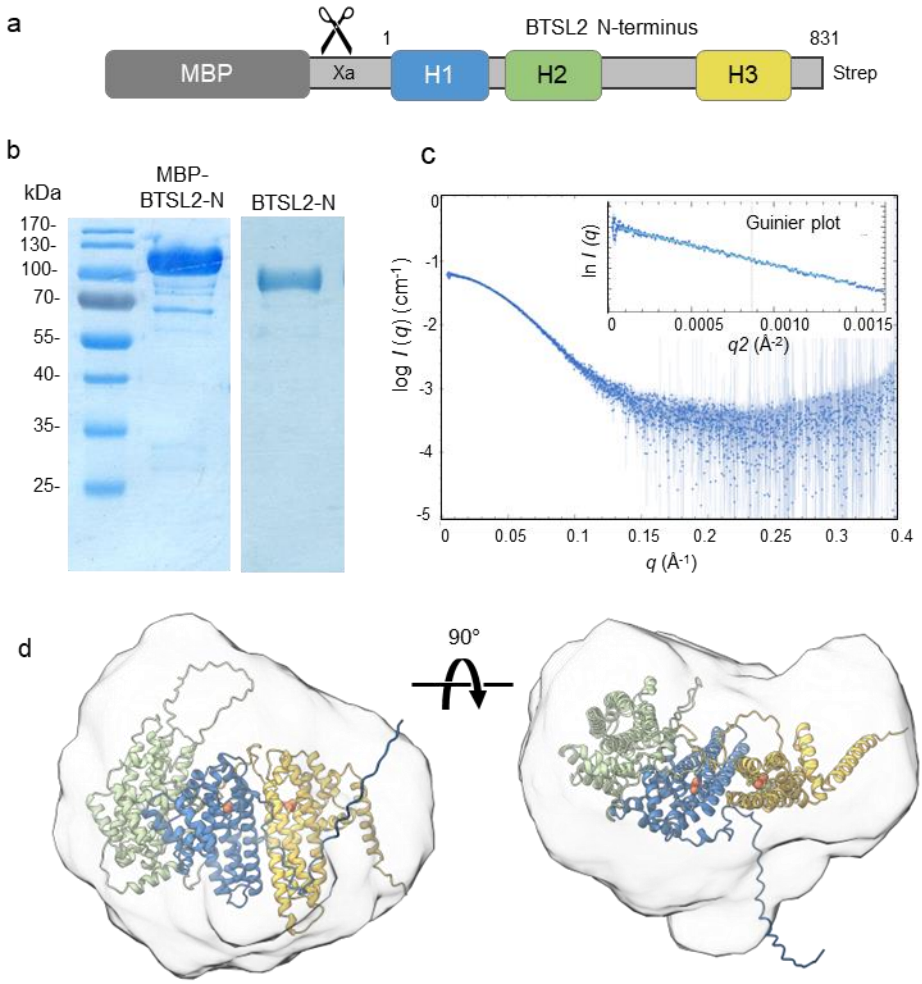

674
675 **Fig. 2 SAXS analysis of the N-terminal domain of BTSL2. a** Expression construct of the Arabidopsis
676 BTSL2 N-terminus (BTSL2-N, codons 1 – 831) encompassing the three Hr-like sequences, flanked by
677 Maltose Binding Protein (MBP) for solubility and a C-terminal Strep tag for affinity purification. **b**
678 Coomassie-stained SDS-PAGE gel of MBP-BTSL2-N purified using Strep-Tactin XT (left) and of BTSL2-
679 N after removal of the MBP domain following protease Xa cleavage and size-exclusion chromatography
680 (right). The images are representative of three experiments. **c** Scattering profile of intensity $I(q)$,
681 presented in log-scale, versus q, the momentum transfer variable which is inversely correlated with the
682 X-ray wavelength in Ångstrom ($Å^{-1}$). Inset: Guinier analysis, in which $\ln(I)$ is plotted against q^2. A radius
683 of gyration Rg of 33.95 ± 0.05 Å was calculated from the slope of the graph ($R^2 = 0.9941$). The intensity
684 at zero angle $I(0)$ was 0.062 cm^{-1} ± 0.000096 and the residual values showed an even distribution. **d**
685 Model of the BTSL2-N protein envelope overlaid with a refined AlphaFold2 model with manually inserted
686 diiron centres. See Supplementary Data 1 for a summary of SAXS experimental data and analysis.
687 Source data have been deposited under accession SASDU79 in www.sasbdb.org.

688

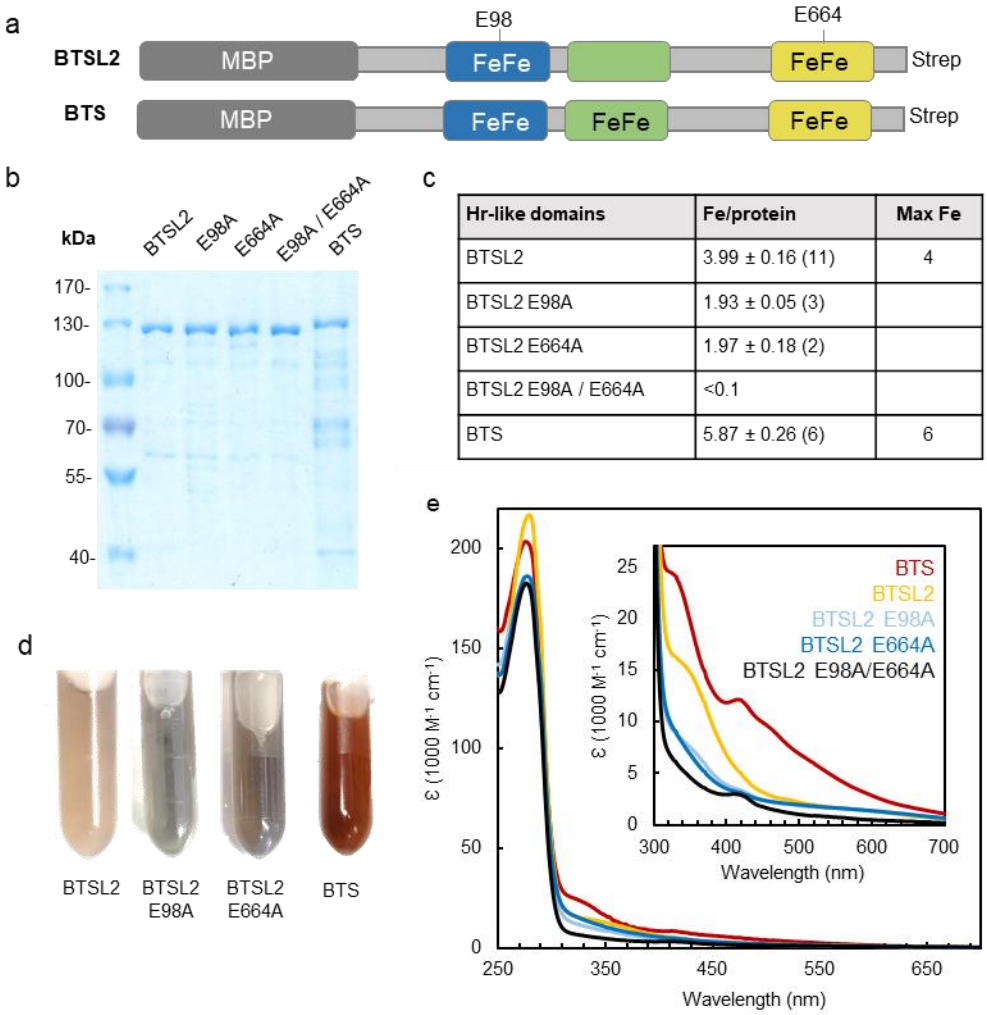

Hr-like domains	Fe/protein	Max Fe
BTSL2	3.99 ± 0.16 (11)	4
BTSL2 E98A	1.93 ± 0.05 (3)	
BTSL2 E664A	1.97 ± 0.18 (2)	
BTSL2 E98A / E664A	<0.1	
BTS	5.87 ± 0.26 (6)	6

689

690

691 **Fig. 3 Iron cofactors in the Hr-like domains of BTSL2 and BTS. a** Diagrams of the MBP fusion
692 proteins of Arabidopsis BTSL2 and BTS N-terminal sequences used for iron quantification and
693 spectroscopy. The E98 and E664 residues are indicated. **b** Coomassie-stained SDS-PAGE gel of the
694 indicated purified proteins including the MBP domain (omitted from the labels), 5 µg protein per lane.
695 The results are representative for the number of preparations given in (c). **c** Quantification of bound iron
696 atoms per polypeptide using the colorimetric chelator Ferene. Values are the mean ± SD of independent
697 protein purifications with n given in brackets. **d-e** Colour (d) and UV-visible spectra (e) of the as-isolated
698 proteins from (a). The protein concentrations were BTSL2, 462 µM; BTSL2 E98A, 345 µM; BTSL2
699 E664A, 527 µM; BTS, 222 µM in (d) and diluted for UV-visible spectroscopy.

700

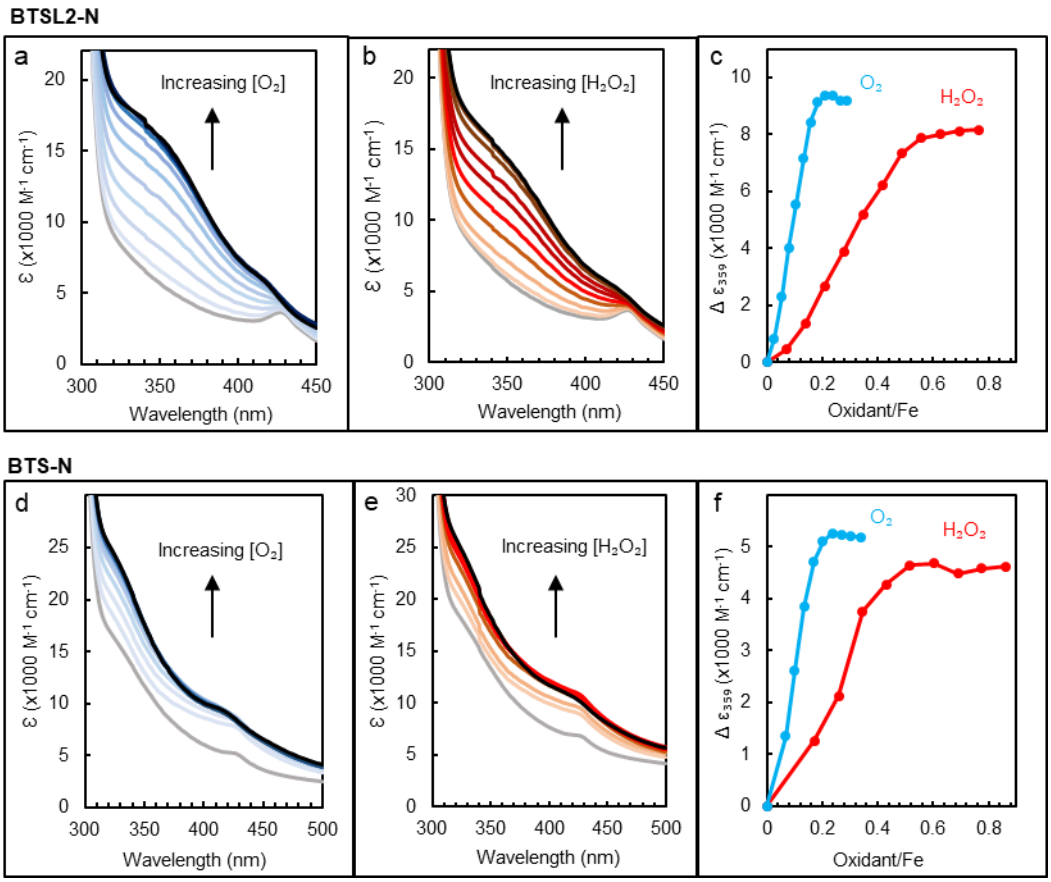

Fig. 4 The Hr-like domains of BTSL2 and BTS are redox-active with O_2 and H_2O_2. Redox titrations monitored by UV-visible absorbance spectroscopy of (**a-b**) BTSL2-N and (**d-e**) BTS-N (MBP fusion proteins, see Fig. 3). Black line: 'as-isolated' proteins purified in air (a, d) or end point of the titration (b, e). Grey line: fully reduced with dithionite in an anaerobic chamber and desalted. Colour lines: titration with O_2 (a and d, blue lines) or H_2O_2 (b and e, orange-red lines). **c, f** The difference in absorbance at 359 nm as a function of the oxidant to iron ratio based on the spectra in (a-b) for BTSL2-N, and spectra in (d-e) for BTS-N.

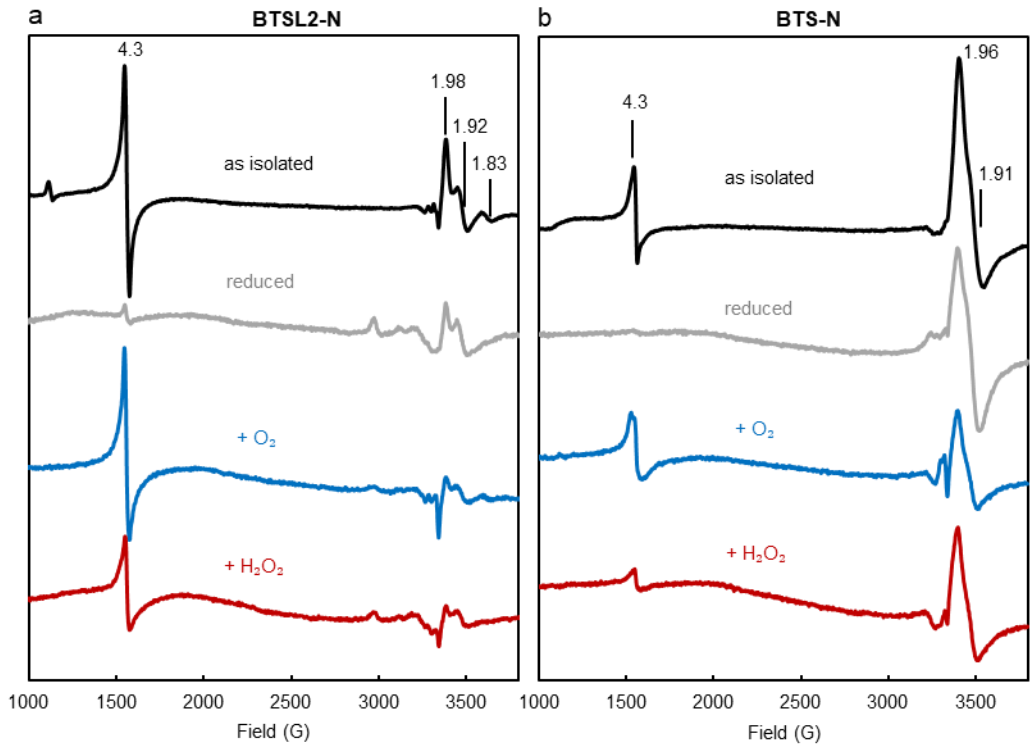

Fig. 5 Analysis of protein-bound iron in the Hr-like domains of BTSL2 and BTS by electron paramagnetic resonance (EPR). EPR spectra of (**a**) BTSL2-N and (**b**) BTS-N. The protein domains were expressed as MBP fusion proteins, see Fig. 3a. The signal with g-value 4.3 is mononuclear iron; the signals with g values around 1.9 are characteristic of a mixed-valent Fe^{2+}/Fe^{3+} centre. Both signals represent ~1% of the protein-bound iron, because the majority of the diiron centres are EPR silent when fully oxidized or reduced. Black: BTSL2-N (287 μM) and BTS-N (222 μM) proteins as isolated. Grey: BTSL2-N (130 μM) and BTS-N (100 μM) reduced with dithionite and desalted in an anaerobic chamber. Blue: BTSL2-N (106 μM) and BTS-N (84 μM) 3 min after mixing with calculated volumes of supersaturated O_2 solution for end concentrations of 216 μM and 262 μM O_2, respectively. Red: BTSL2-N (106 μM) and BTS-N (84 μM) 3 min after mixing with 216 μM and 262 μM H_2O_2, respectively. Spectra were adjusted to compensate for dilution by reagent additions and desalting. EPR spectra were recorded at 10 K using the following parameters: microwave frequency ν_{MW} = 9.353 GHz, modulation frequency ν_M = 100 kHz, microwave power P_{MW} = 3.17 mW, modulation amplitude A_M = 5 G. The results are representative of two independent protein preparations.

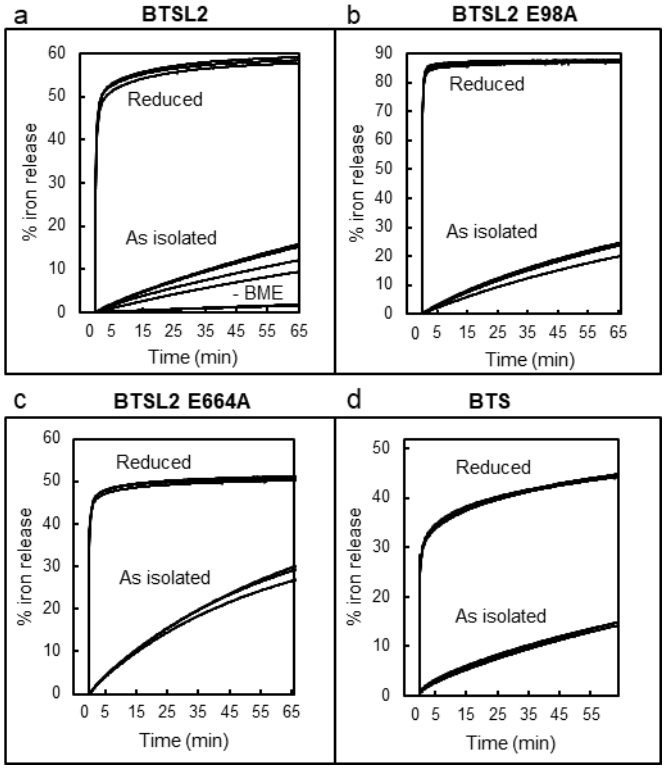

Fig. 6 Iron binding to the Hr-like domain depends upon oxidation state. a-d Release of protein-bound iron monitored using the colorimetric iron chelator Ferene. An increase in absorbance over time was correlated with the amount of iron released from the protein. Traces of independent time course measurements are overlaid. The 'as isolated' proteins are in the predominantly oxidized form but contain residual β-mercaptoethanol (BME) included to stabilize BTS. For BTSL2-N, protein isolated without BME is also shown. Proteins were reduced following incubation with dithionite and desalting. (**a**) BTSL2-N; (**b**) BTSL2-N E98A; (**c**) BTSL2-N E664A; (**d**) BTS-N.

736

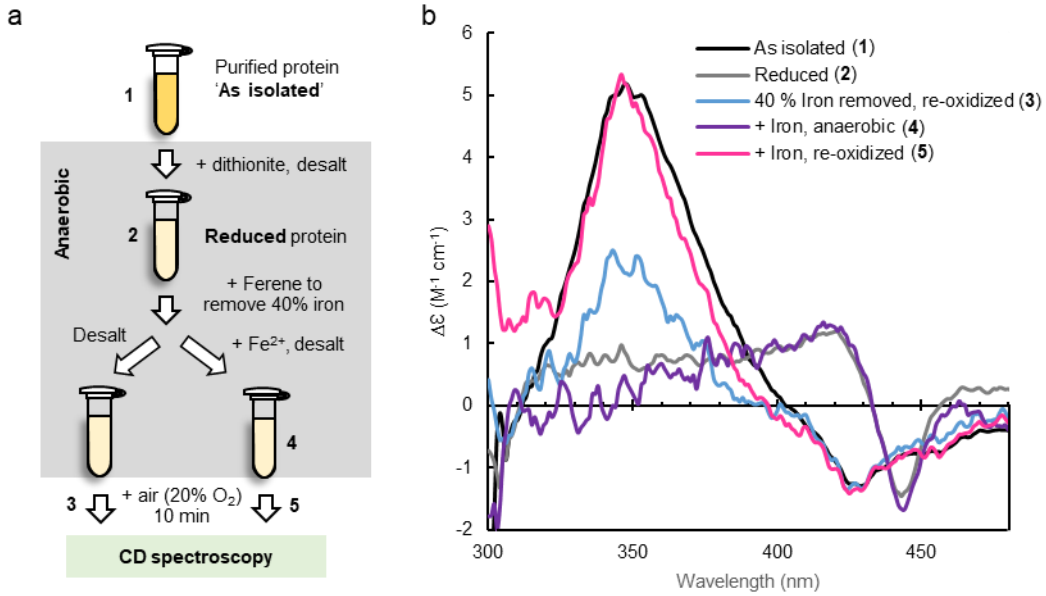

737

738 **Fig. 7 BTSL2-N can be fully reconstituted after partial iron removal. a** Diagram of the experimental
739 procedures to first remove labile iron and then reconstitute the diiron centres monitored by CD
740 spectroscopy, which only detects protein-bound iron. **b** CD spectra of purified MBP-BTSL2-N (86 μM)
741 as isolated (black) and after reduction with dithionite and its subsequent removal by desalting (grey).
742 The reduced protein was mixed with a defined amount of Ferene, calculated to remove 40% of the
743 protein-bound iron. Half the sample was desalted to remove Fe^{2+} chelator species, and exposed to O_2
744 (light blue) to demonstrate the partial removal of protein-bound iron. The other half was mixed with a 3-
745 fold excess of ferrous ammonium sulfate and desalted to remove unbound iron, keeping the protein
746 reduced (purple), followed by exposure to O_2 (magenta). Spectra were adjusted to compensate for
747 dilution by reagent additions and desalting. The results are representative of two independent
748 experiments.

749

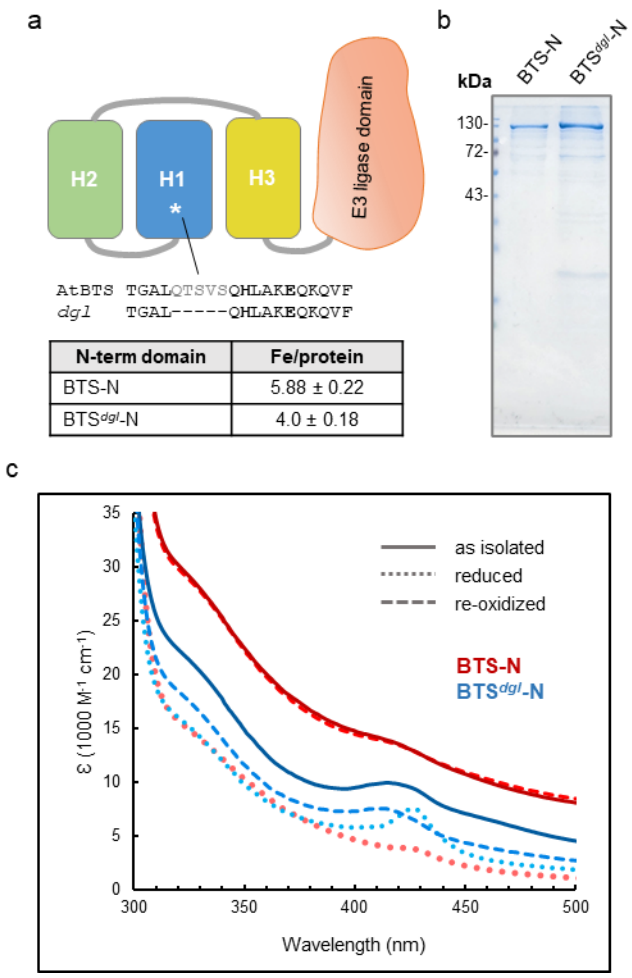

N-term domain	Fe/protein
BTS-N	5.88 ± 0.22
BTS^{dgl}-N	4.0 ± 0.18

Fig. 8 Lack of iron binding to H1 affects oxidation of the diiron centres and activity of BTS in vivo. a Diagram of the position of the 5 amino acid deletion in the *dgl* variant protein of BTS. The mutation identified in the *BTS* homologue in pea[33], causing mis-regulation of iron homeostasis, was reconstructed in the Arabidopsis (At) expression construct of the N-terminal domain (BTS-N). The deletion is adjacent to two of the iron-binding ligands, H173 and E177, shown in bold. **b** Coomassie-stained SDS-PAGE gel of purified BTS-N (2.5 µg) and the *dgl* variant protein BTS^{dgl}-N (5 µg), expressed as MBP fusion proteins in *E. coli*. The experimentally determined iron:protein ratio was 4 ± 0.18 for BTS^{dgl}-N. **c** Redox reactions monitored by UV-visible spectroscopy of BTS^{dgl}-N (blue-shaded lines) and BTS-N (red-shaded lines, from Fig. 3d) for comparison. The as-isolated proteins (solid lines) were reduced with dithionite (dotted lines) and re-oxidized by exposure to air for 50 min (dashed lines). Iron:protein rations and spectra of BTS^{dgl}-N are representative of two independent protein purifications.

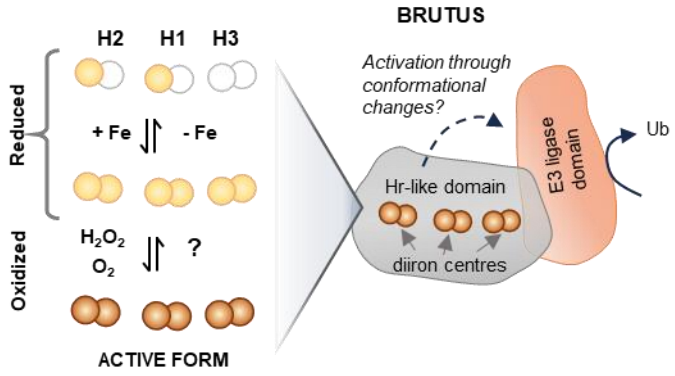

764
765
766 **Fig. 9 Proposed mechanism by which BTS/Ls are activated by iron binding and oxidation.**
767 In a reducing cell environment, iron binding is dynamic, with the diiron centres becoming fully occupied
768 as the iron concentration increases. Oxidation of the diiron centres increases the binding affinity of iron,
769 fixing the cofactors in place and leading to activation of the E3 ubiquitin ligase, presumably through
770 conformational changes. Depicted here is the model for BTS with three diiron centres; the H2 diiron
771 centre is missing in BTSL2. Fe^{2+} and Fe^{3+} are indicated by light brown and darker brown spheres,
772 respectively.

773